CHAPTER 6

EFFECT OF ULTRASONIC SHOT PEENING ON LCF BEHAVIOR OF Ti–6Al–4V ALLOY

6.1 INTRODUCTION

This chapter presents the effect of ultrasonic shot peening (USSP) on tensile and low cycle fatigue (LCF) behavior of the alloy Ti–6Al–4V at room temperature. The results are discussed in terms of increase in the resistance of the material against crack initiation due to grain refinement in the surface region and the associated compressive stresses resulting from USSP, in particular at the lower strain amplitudes. USSP was carried out in gage section of the cylindrical specimens, with hard steel balls of 3 mm diameter for 5 minute, to modify the surface. Nanostructure of 17 to 25 nm was developed in surface region of the alloy Ti–6Al–4V. Some of the USSPed samples were also subjected to stress relieving (SR) treatment at 300 and 400 °C for 1h. Strain controlled LCF tests were conducted on the non-USSPed, USSPed and USSPed+SR samples, at different total strain amplitudes of ±0.60%, ±0.65%, ±0.70%, ±0.75%, ±0.80%, ±0.90%, and ±1.0%. Some LCF tests were also conducted at total strain amplitude of ±0.75%, on the samples USSPed for 2.5 and 7.5 minute.

Fatigue life of the USSPed samples was found to increase progressively with decrease in total strain amplitude to much larger extent in comparison with those of the non-USSPed samples. Fatigue life of the USSPed sample at the lowest total strain amplitude of ±0.6% was enhanced by four times that of the non-USSPed one. The enhanced fatigue life of the USSPed samples was reduced following the stress relieving

treatment (400 °C for 1h) but was higher than that of the non-USSPed one. There was cyclic softening from beginning till the failure at the high strain amplitudes ($\Delta\varepsilon_t/2 \geq \pm 0.75\%$) whereas cyclic hardening was exhibited during the initial 100 cycles and was followed by softening at the lower strain amplitudes ($\Delta\varepsilon_t/2 \leq \pm 0.70\%$). Deformation structure of the non-USSPed, USSPed and USSPed+SR samples, tested at different strain amplitudes was analysed.

6.2 TENSILE BEHAVIOR

6.2.1 Effect of USSP on Tensile Properties

Effect of surface nanostructure on tensile properties of the alloy Ti–6Al–4V was studied at room temperature for the specimens USSPed for 5 and 7.5 minutes. Tensile engineering stress-strain curves of the non-USSPed and USSPed specimens are shown in Fig. 6.1.

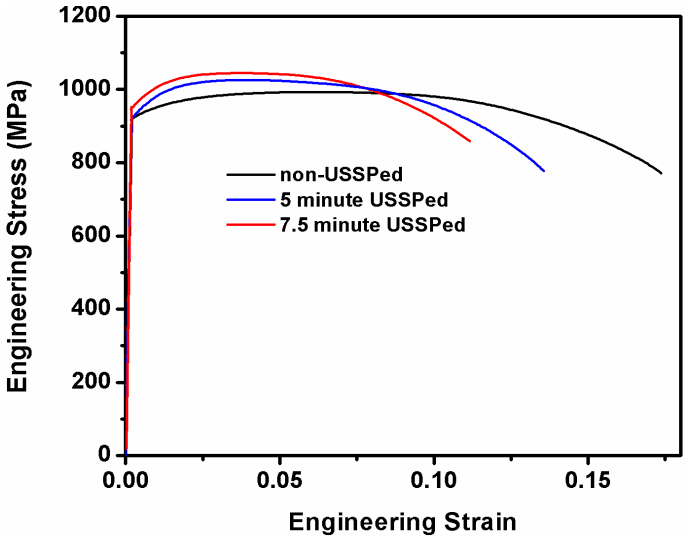

Fig. 6.1 Tensile engineering stress-strain curves of the non-USSPed and USSPed samples.

It was observed from Fig. 6.2 that yield strength (YS) increased from 907 MPa to 940 MPa and the ultimate tensile strength (UTS) increased from 997 MPa to 1044 MPa following USSP.

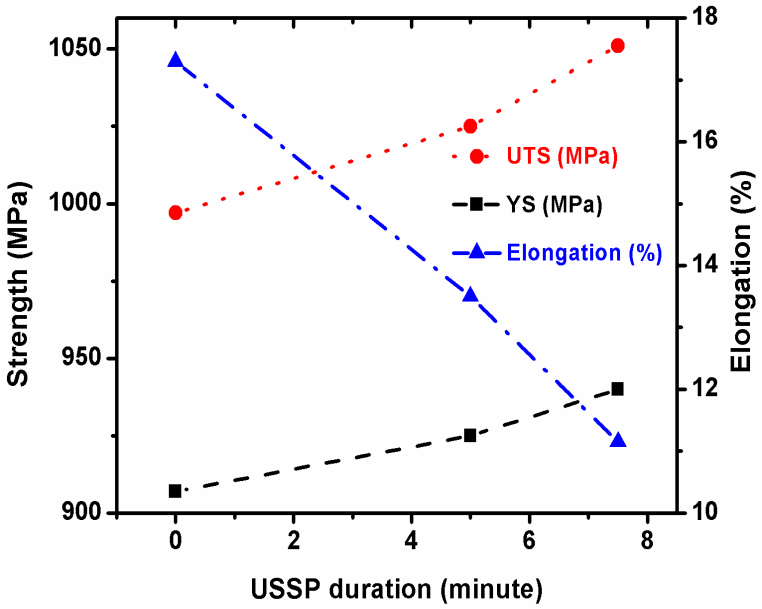

Fig. 6.2 Variation of yield strength, tensile strength and elongation with the duration of USSP.

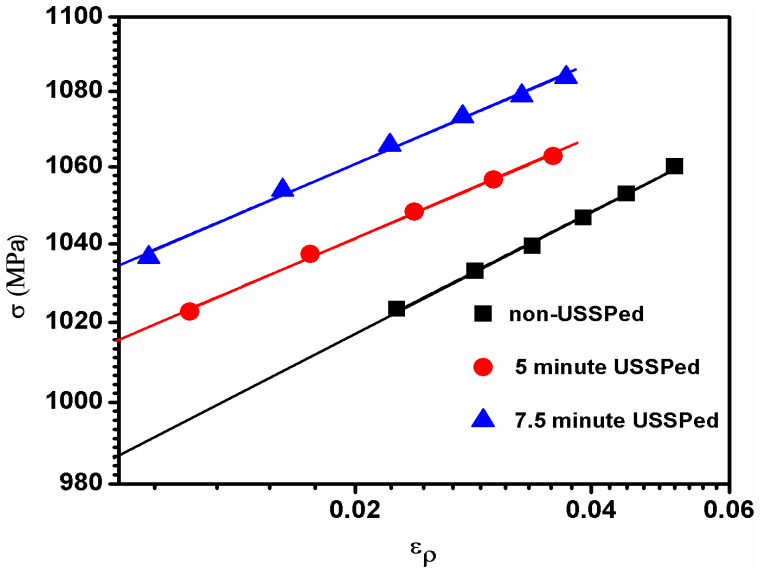

Fig. 6.3 The true stress (σ) vs true plastic strain (ε_ρ) plot on log scale showing work-hardening behavior of the non-USSPed and USSPed specimens.

The log-log plot of the true stress vs true plastic strain is shown in Fig. 6.3. The strain hardening exponent (n) was determined from the slopes of the plots and the strength coefficient (K) was determined from the intercept on y axis at ε_ρ=1, based on the equation $\sigma = K\varepsilon_\rho^n$ [Hollomon (1945)]. The value of *n* for the non-USSPed sample was 0.044 while the values were found to be lower for the specimens USSPed for 5 and 7.5 minute as 0.040, 0.035 respectively. Table 6.1 summarises the tensile test results of the USSPed samples.

Table 6.1 Effect of ultrasonic shot peening on tensile properties.

S. No.	USSP duration (minute)	YS (MPa)	UTS (MPa)	Elongation (%)	n	K (MPa)
1.	0	907	997	17.10	0.044	1210
2.	5	925	1025	13.52	0.040	1170
3.	7.5	940	1044	11.13	0.035	1150

6.2.2 Fracture Behavior of Tensile Tested Specimens

Fracture surfaces of the tensile tested samples were examined using scanning electron microscope. Ductile fracture was observed in all the conditions. It may be seen from these fractographs that well defined dimples are there in the specimens, non-USSPed and USSPed, tested at room temperature (Fig. 6.4).

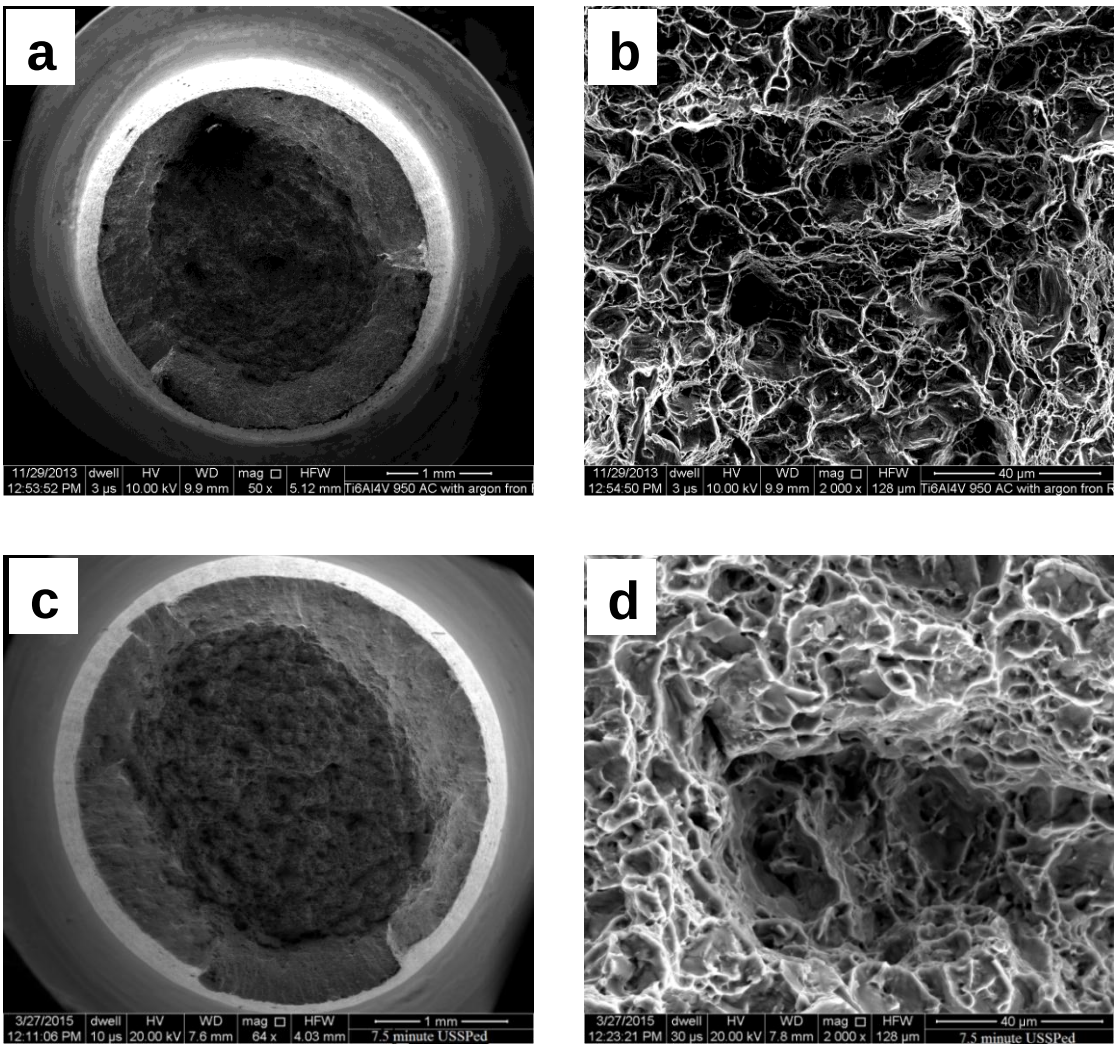

Fig. 6.4 Fracture surface of the tensile tested specimens: (a, b) non-USSPed and (c, d) USSPed for 7.5 minutes.

6.3 LOW CYCLE FATIGUE BEHAVIOR

Strain controlled tests were conducted at ±0.75% strain amplitude on the 2.5, 5 and 7.5 minute USSPed samples to examine LCF behavior. It was found that the LCF life was higher for the 5 minute USSPed sample (Fig. 6.5) in comparison to those of the 2.5 and 7.5 minute USSPed samples because the compressive residual stress was lower for the 2.5 minute and the surface roughness was higher for the 7.5 minute USSPed sample

than that of the 5 minute USSPed sample (as discussed in Chapter 3). It is well known that roughness and compressive residual stress play important roles on LCF life.

The enhanced fatigue life from the USSP was reduced due to stress relieving treatment at the both 300 °C and 400 °C. Reduction in LCF life was more due to stress relieving treatment at 400 °C than that at 300 °C. It may be seen from Chapter 3 (Fig. 3.15) that compressive residual stress was increased with USSP duration. However, the compressive stress was reduced due to stress relieving treatment. Hence, reduction in LCF life due to SR treatment may be understood.

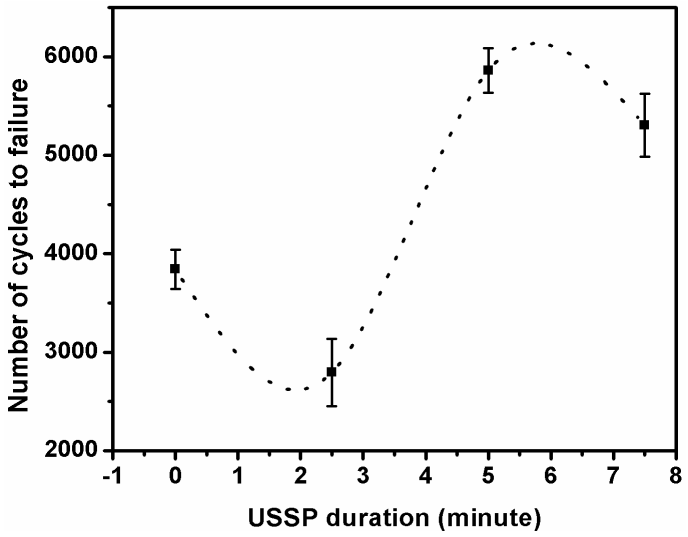

Fig. 6.5 Variation of LCF life with duration of USSP at constant strain amplitude of ±0.75%.

Table 6.2 Effect of stress relieving treatment on LCF life of USSPed sample.

USSP duration (minute)	**$\Delta\varepsilon_t/2$ (%)**	**Stress relieving treatment (°C)**	**Fatigue life (N)**
5	±0.75	300	5645±257
5	±0.75	400	5400±349

LCF tests were conducted on the 5 minute USSPed, 5 minute USSPed+SR and the non-USSPed samples, under identical test conditions at different total strain amplitudes of ±0.60%, ±0.65%, ±0.70%, ±0.75%, ±0.80%, ±0.90% and ±1.0%, at room temperature. The variations of average cyclic stress (Δσ/2) with number of cycles (N), at different total strain amplitudes are shown in the Figs. 6.6a, 6.6b and 6.6c for the non-USSPed, 5 minute USSPed and the USSPed+SR samples respectively.

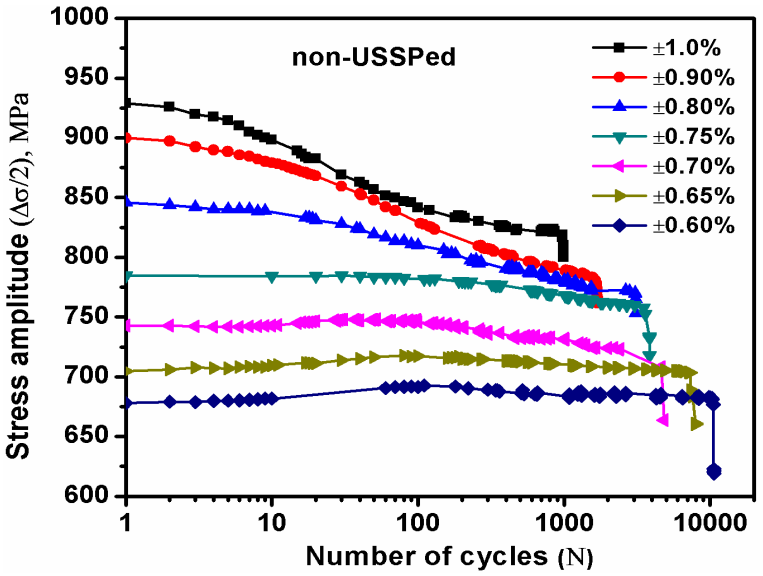

(a)

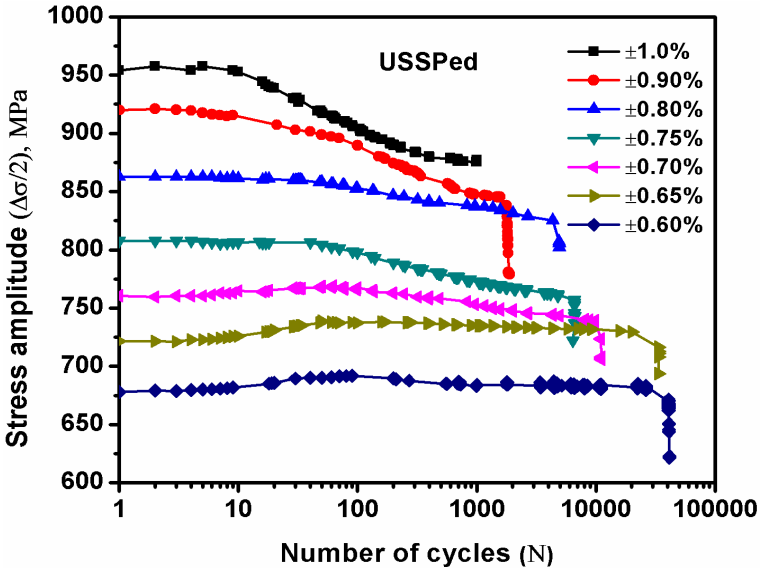

(b)

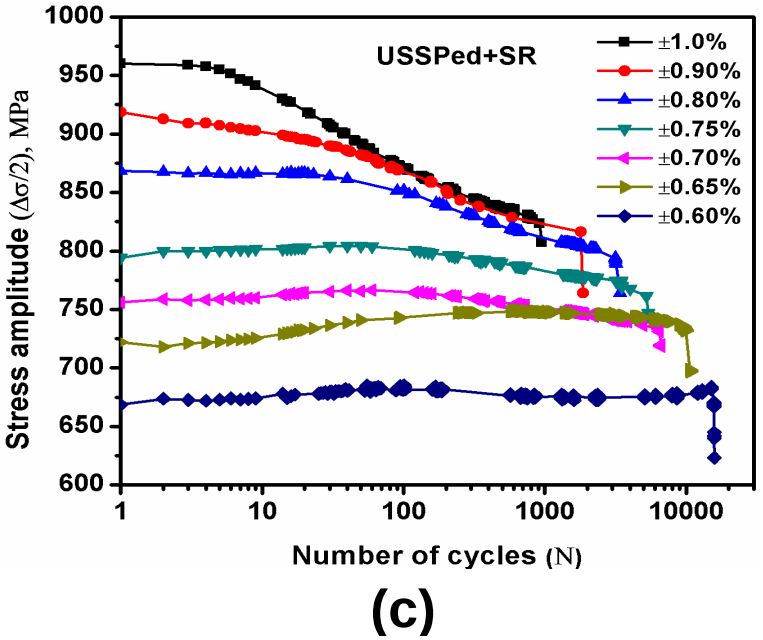

Fig. 6.6 Variation of cyclic stress amplitude with number of cycles at different total strain amplitudes at strain rate of $5\times10^{-3}s^{-1}$: (a) non-USSPed, (b) USSPed for 5 minute and (c) USSPed+SR.

There was continuous cyclic softening from the beginning till failure at the higher strain amplitudes (≥±0.75% to ±1.0%). However, cyclic hardening was observed approximately up to the initial 100 cycles and was followed by softening till fracture, at the lower strain amplitudes (±0.60% to ±0.70%) for all the conditions (non-USSPed, USSPed and USSPed+SR). LCF life in the non-USSPed, USSPed and USSPed+SR condition was analysed using the Coffin-Manson relationship between the plastic strain amplitude ($\Delta\varepsilon_p/2$) and number of reversals to failure ($2N_f$) [Dieter (1988)].

$$\Delta\varepsilon_p/2 = \varepsilon'_f (2N_f)^c \quad \ldots\ldots\ldots\ldots\ldots\ldots\ldots\ldots\ldots\ldots\ldots\ldots \quad (6.1)$$

where ε'_f and c are fatigue ductility coefficient and exponent respectively.

Coffin-Manson plots of log ($\Delta\varepsilon_p/2$) vs log ($2N_f$) are shown in Fig. 6.7. The numerical values of ε'_f and c are recorded in Table 6.3.

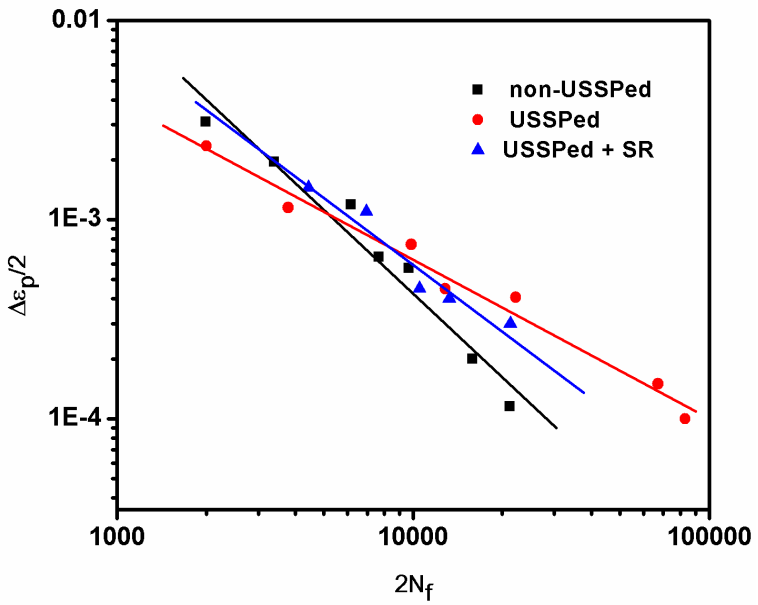

Fig. 6.7 Coffin-Manson plot showing variation of fatigue life as number of reversals to failure ($2N_f$) with plastic strain amplitude, at strain rate of $5\times10^{-3}s^{-1}$.

It is obvious from Fig. 6.7 that fatigue life of the USSPed specimens progressively increased with decrease in strain amplitude. The increase in fatigue life was much larger in the as USSPed than those in the non-USSPed and the USSPed+SR conditions. While fatigue life of the USSPed specimen was nearly comparable to that of the non-USSPed sample at the highest strain amplitude of ±1.0%, it was increased by nearly four times at the lowest strain amplitude of ±0.60%. However, the enhanced fatigue life resulting from USSP decreased following the stress relieving treatment. The enhanced fatigue life of the USSPed specimen reflects the beneficial effect of surface grain refinement and the associated compressive stress in the surface region on fatigue resistance.

Table 6.3 Numerical values of LCF parameters of non-USSPed and USSPed samples, tested at room temperature.

Conditions	Fatigue ductility coefficient (ε'_f)	Fatigue ductility exponent (c)
non-USSPed	41.869	-1.241
USSPed	3.588	-0.934
USSPed+SR	6.572	-1.017

6.3.1 Fracture Behavior of LCF Tested Specimens

Fracture behavior of the non-USSPed, 5 minute USSPed and 5 minute USSPed+SR LCF specimens tested at strain amplitudes of ±0.60%, ±0.65%, ±0.75%, ±0.80% and 1.0% are shown in Figs. 6.8, 6.9, 6.10, 6.11 and 6.12 respectively. Similar fracture morphology was observed for the non-USSPed, USSPed and USSPed+SR conditions with multiple crack initiation sites, at ±0.60%, ±0.80% and ±1.0% strain amplitudes (Figs. 6.8, 6.11 and 6.12).

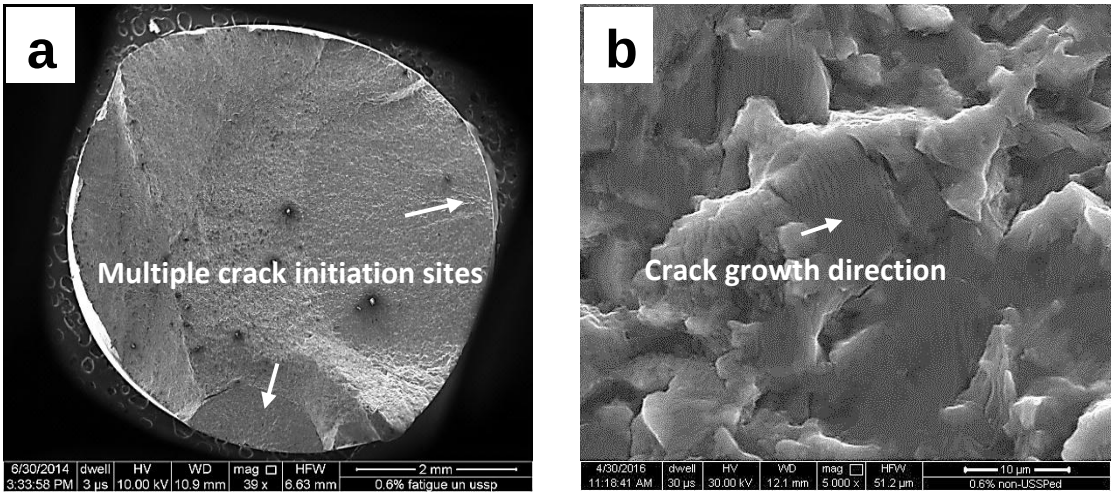

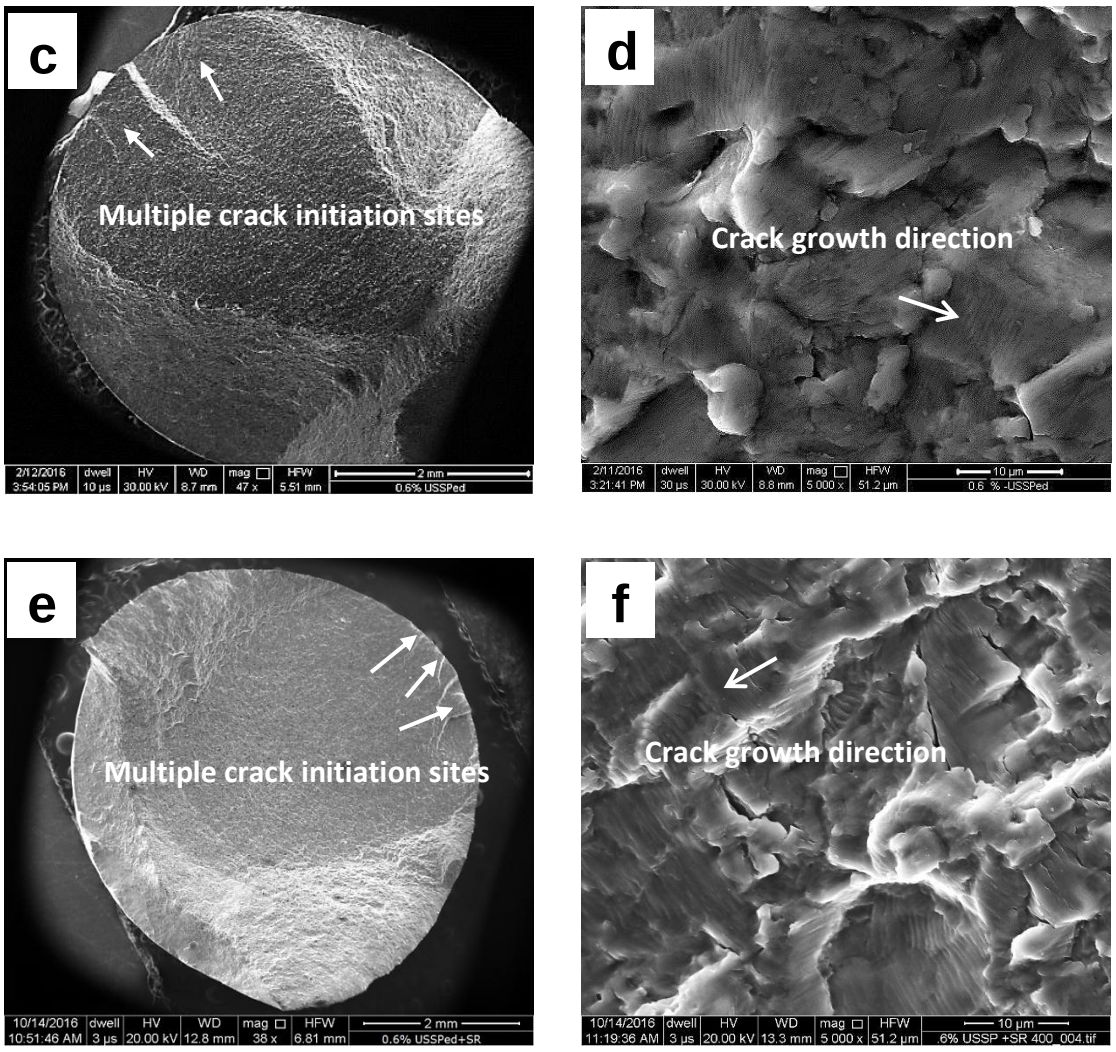

Fig. 6.8 Fractographs showing fracture surfaces of the specimens tested in LCF at ±0.60% strain amplitude: (a, b) non-USSPed, (c, d) USSPed and (e, f) USSPed+SR.

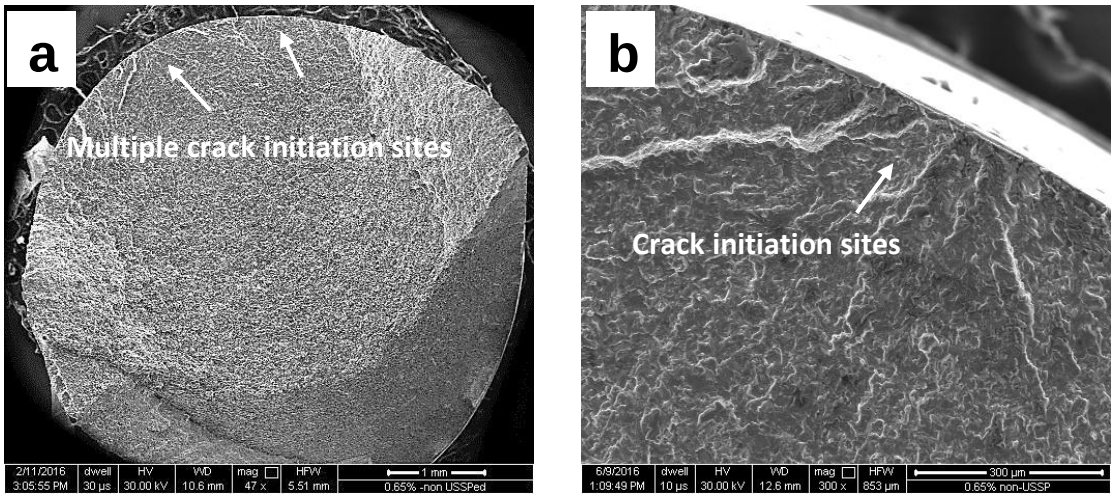

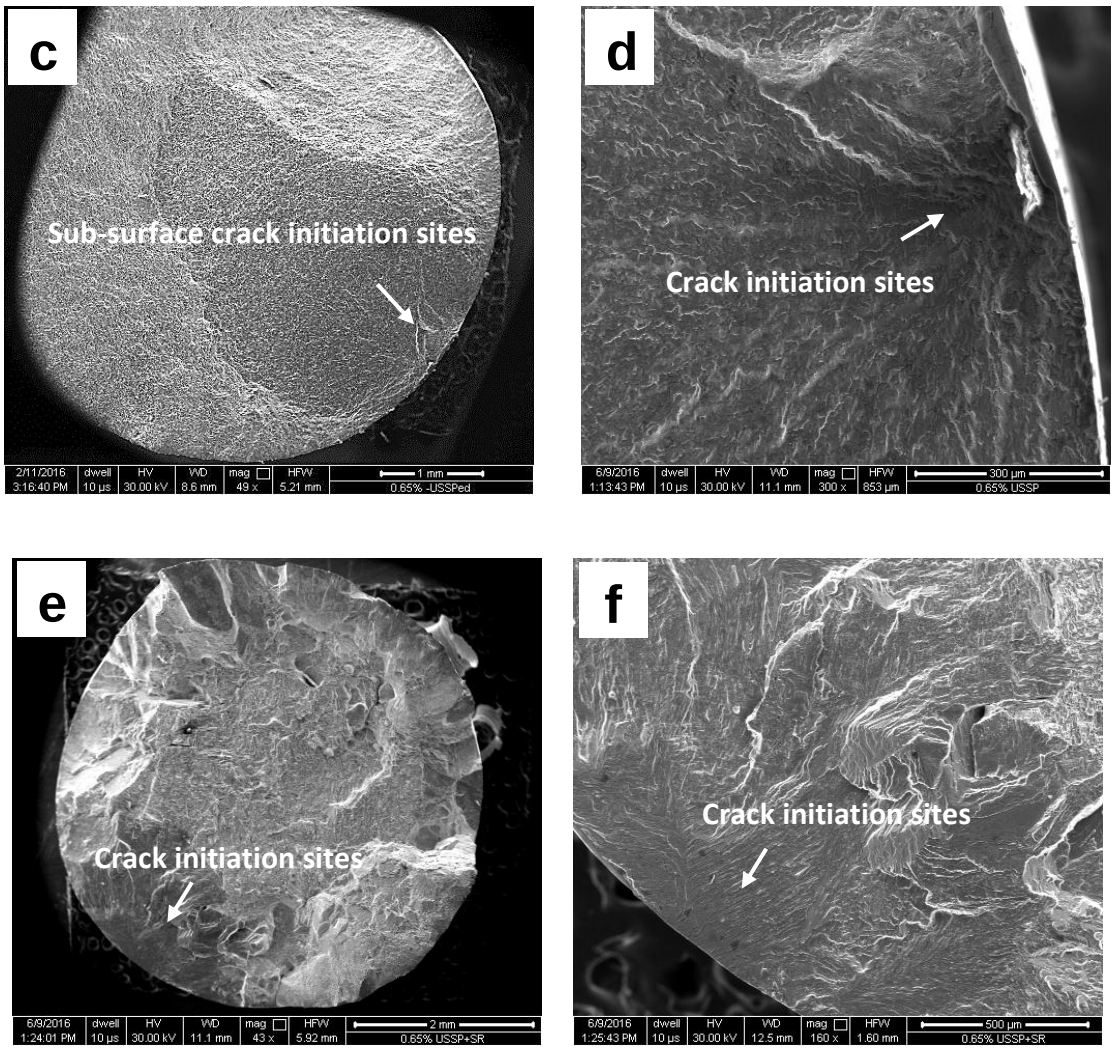

Fig. 6.9 Fractographs showing fracture surface of the LCF specimens tested at ±0.65% strain amplitude: (a, b) non-USSPed, (c, d) USSPed and (e, f) USSPed+SR.

However, sub-surface fatigue cracks were observed in the USSPed sample tested at ±0.65% strain amplitude and striations were observed just after ≈400 μm depth from the surface (Fig. 6.9d). Facets were observed on fracture surface of the USSPed+SR sample (Fig. 6.9e). Initiation of multiple cracks may be seen in all the conditions in different regions of the fractured surfaces in different orientations, propagated to varying depths.

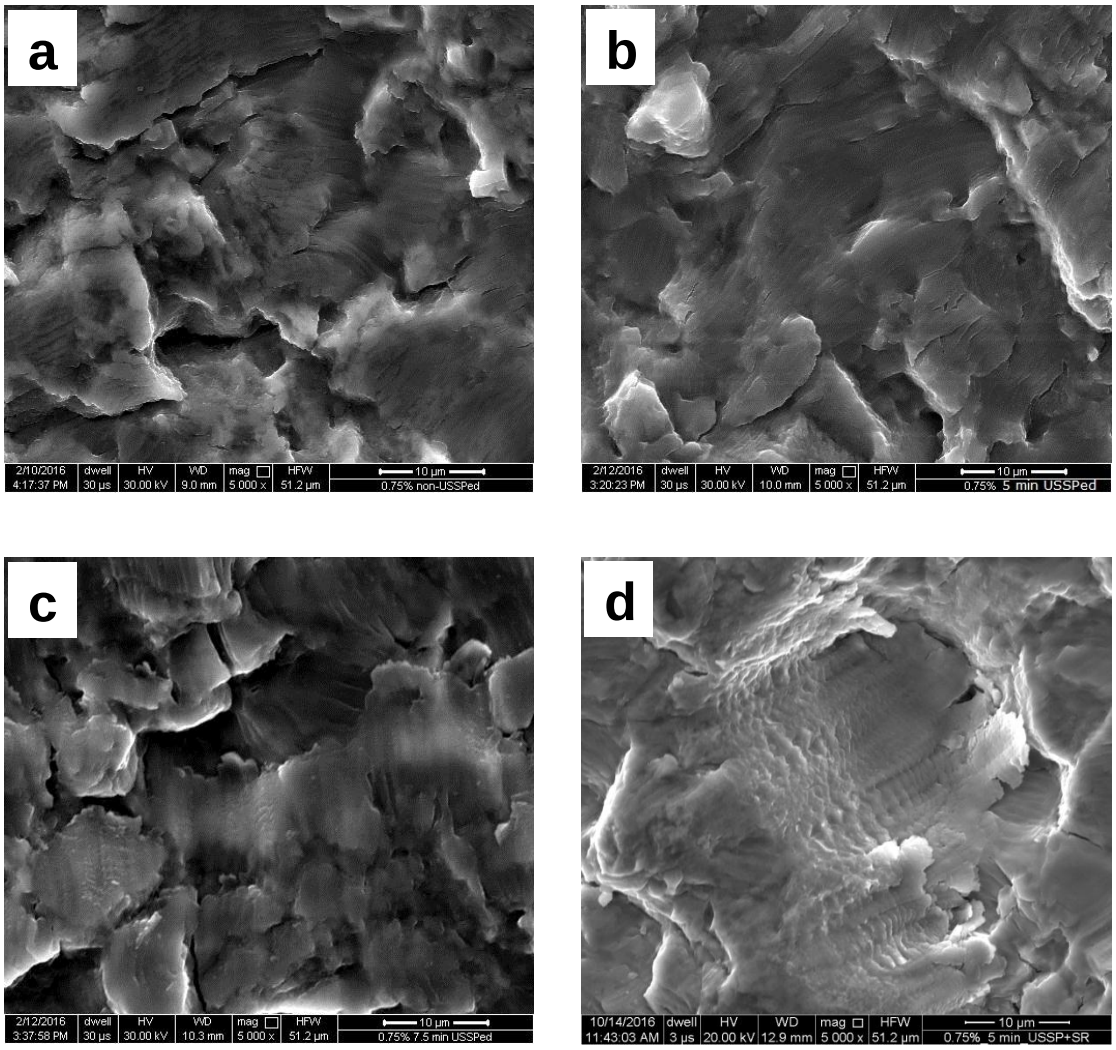

Fig. 6.10 Fractographs showing fracture surfaces of the specimens tested at ±0.75% strain amplitude: (a) non-USSPed, (b) 5 minute USSPed, (c) 7.5 minute USSPed and (d) 5 minute USSPed+SR.

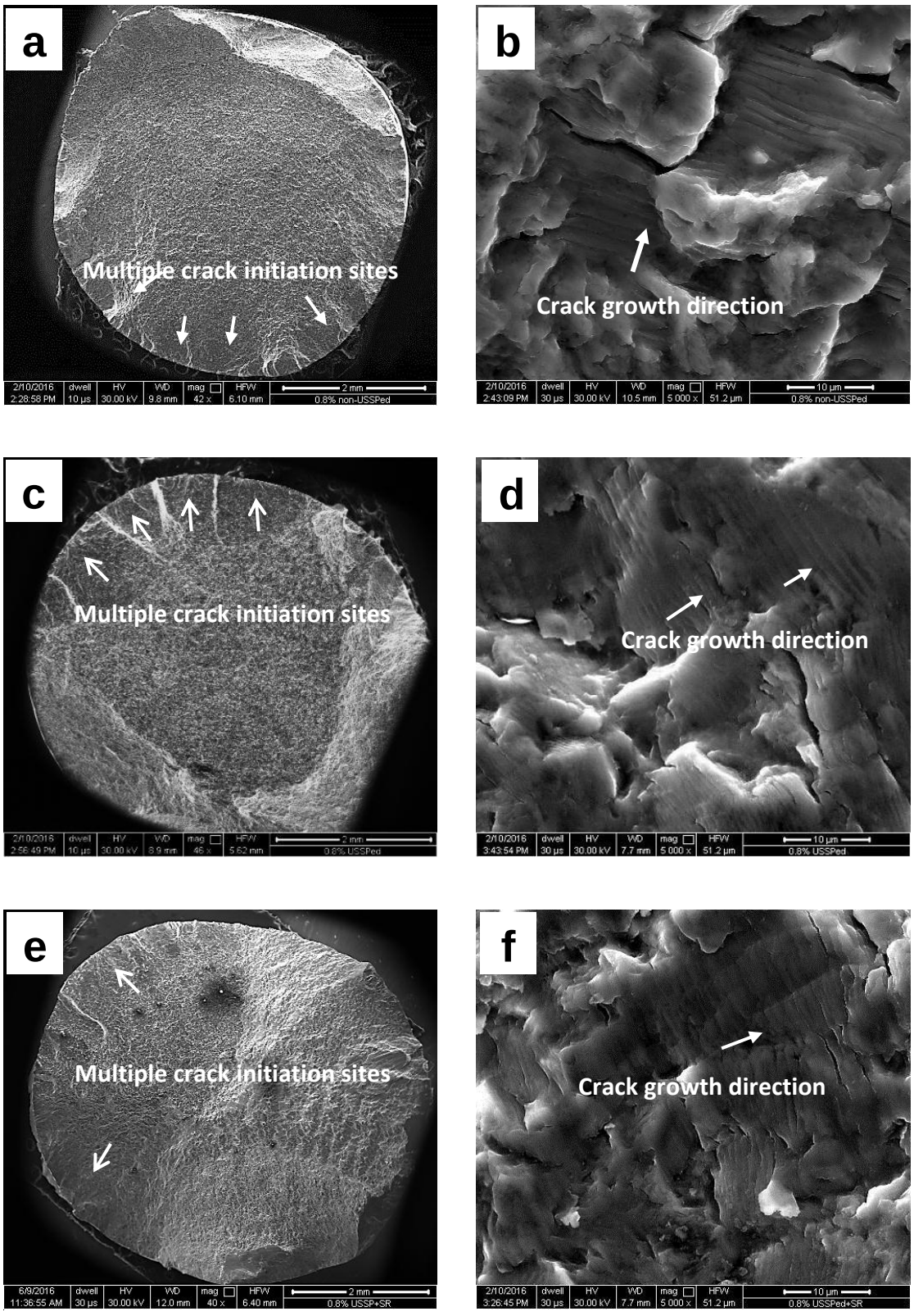

Fig. 6.11 Fractographs showing fracture surfaces of the specimens tested in LCF at ±0.80% strain amplitude: (a, b) non-USSPed, (c, d) USSPed and (e, f) USSPed+SR.

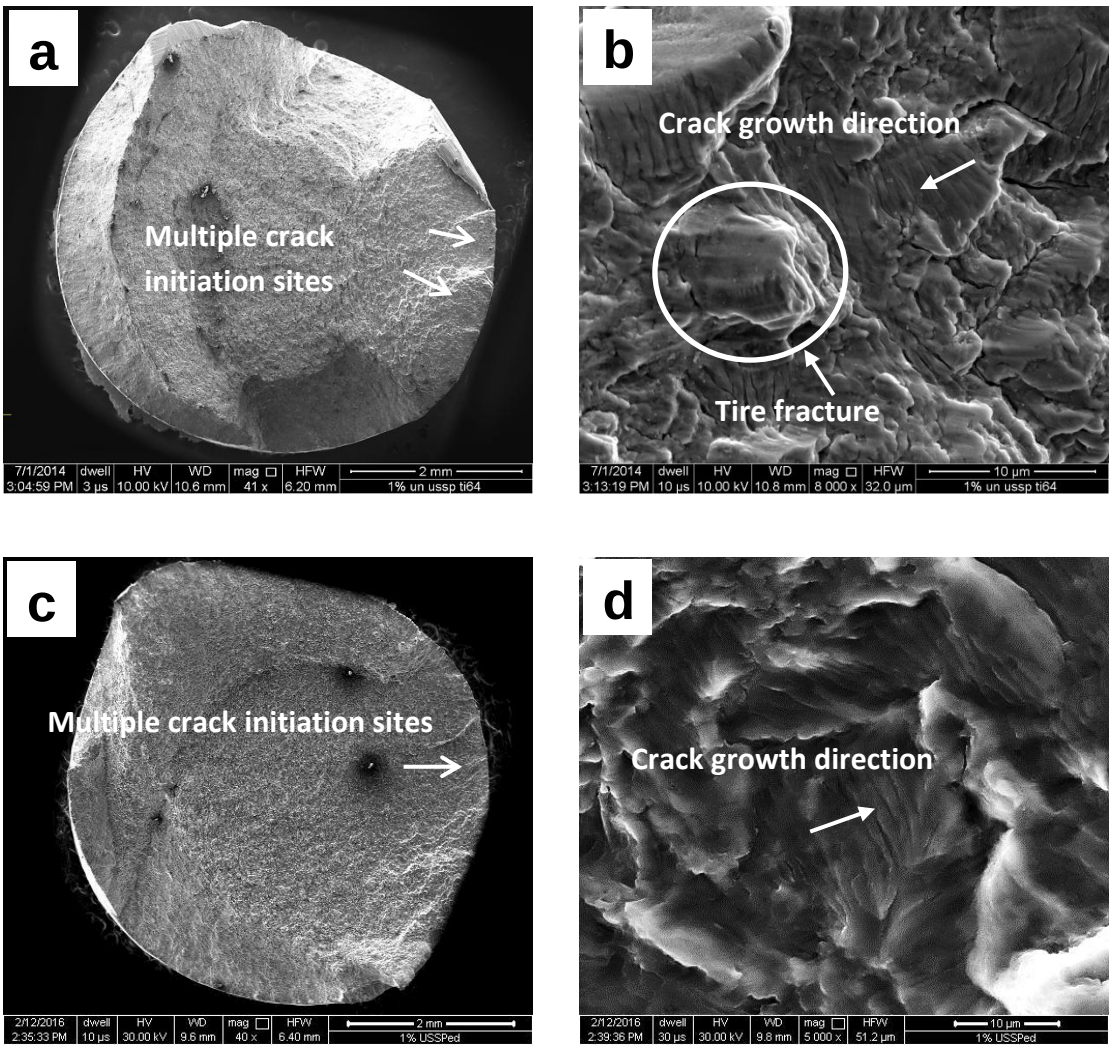

Fig. 6.12 Fractographs showing fracture surfaces of the specimens tested at ±1.0% strain amplitude: (a, b) non-USSPed and (c, d) USSPed.

Tire fracture was observed on fracture surface of the sample USSPed for the 7.5 minute and 5 minute USSPed+SR conditions, tested at ±0.75% strain amplitude. It may be seen in Fig. 6.12 that inter-striation spacing was approximately same because there was no change in LCF life at ±1.0% strain amplitude. Tire fracture was observed also in the non-USSPed sample tested at ±1.0% strain amplitude.

However, there was a marked difference in fatigue crack propagation of the non-USSPed, USSPed and USSPed+SR specimens, as revealed by the inter-striation

spacings. Distinct fatigue striations were observed in stage II fatigue crack propagation in the three conditions; the non-USSPed, USSPed and USSPed+SR, as shown in Figs. 6.8 (b, d, f); 6.9 (b, d, f); 6.10 (b, d); 6.11 (b, d, f) and 6.12 (b, d) respectively, tested at different strain amplitudes. The inter-striation spacing was relatively less in the case of USSPed samples than those in the USSPed+SR and non-USSPed samples, under identical test conditions. The number of cycles spent in the process of crack propagation (N_p) was determined, counting the number of fatigue striations over the largest region of the fracture surface resulting from fatigue. The number of cycles spent in the process of crack initiation (N_i) was estimated from the difference between the number of cycles to failure (N_f) and the number of cycles spent in crack propagation (N_p). The variation of N_i and N_p with total strain amplitude is shown in Fig. 6.13.

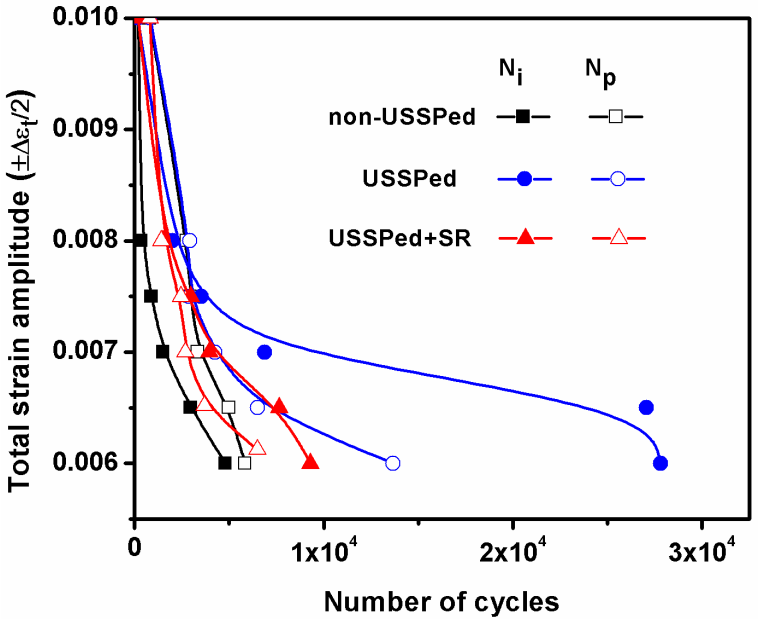

Fig. 6.13 Variation of number of cycles for crack initiation (N_i) and crack propagation (N_p) of the non-USSPed, 5 minute USSPed and USSPed+SR samples, fractured in LCF at strain rate of $5\times10^{-3}s^{-1}$.

6.3.2 Deformation Behavior in LCF

Transmission electron microscopy based structural analysis was carried out to examine deformation behaviour of the LCF tested samples at total strain amplitudes of ±0.60%, ±0.65%, ±0.70% and ±0.80% on non-USSPed, USSPed and USSPed+SR samples, are shown in Figs. 6.14, 6.15, 6.16 and 6.17. The deformation behavior indicates typical dislocations activity resulting from LCF. The dislocation structures of USSPed samples were quite different from those of the non-USSPed samples at low and high strain amplitudes. Dislocation pile-ups were observed at strain amplitudes of ±0.60% and ±0.65% in the non-USSPed condition.

Dislocation pile-ups as indicated by arrows were observed near boundaries of secondary α (Figs 6.14a and 6.15a) [Rao et al. (2013)]. Narrow dislocation and planar defects may be seen in Fig. 6.14c and 6.14e, resulting from LCF at ±0.60% strain amplitude, in USSPed and USSPed+SR conditions respectively.

Figure 6.15c shows individual dislocations (shown by arrow), tested at low strain amplitude of ±0.65% in the USSPed condition resulting from higher fatigue life. Individual dislocations were reported in the alloy IMI 834, fatigue tested at room temperature at strain amplitude of ±0.8% [Singh et al. (2002)]. However, multiple arrayed planar defects may be observed in the USSPed+SR sample, tested at ±0.65% strain amplitude, in the secondary α region (Fig. 6.15e).

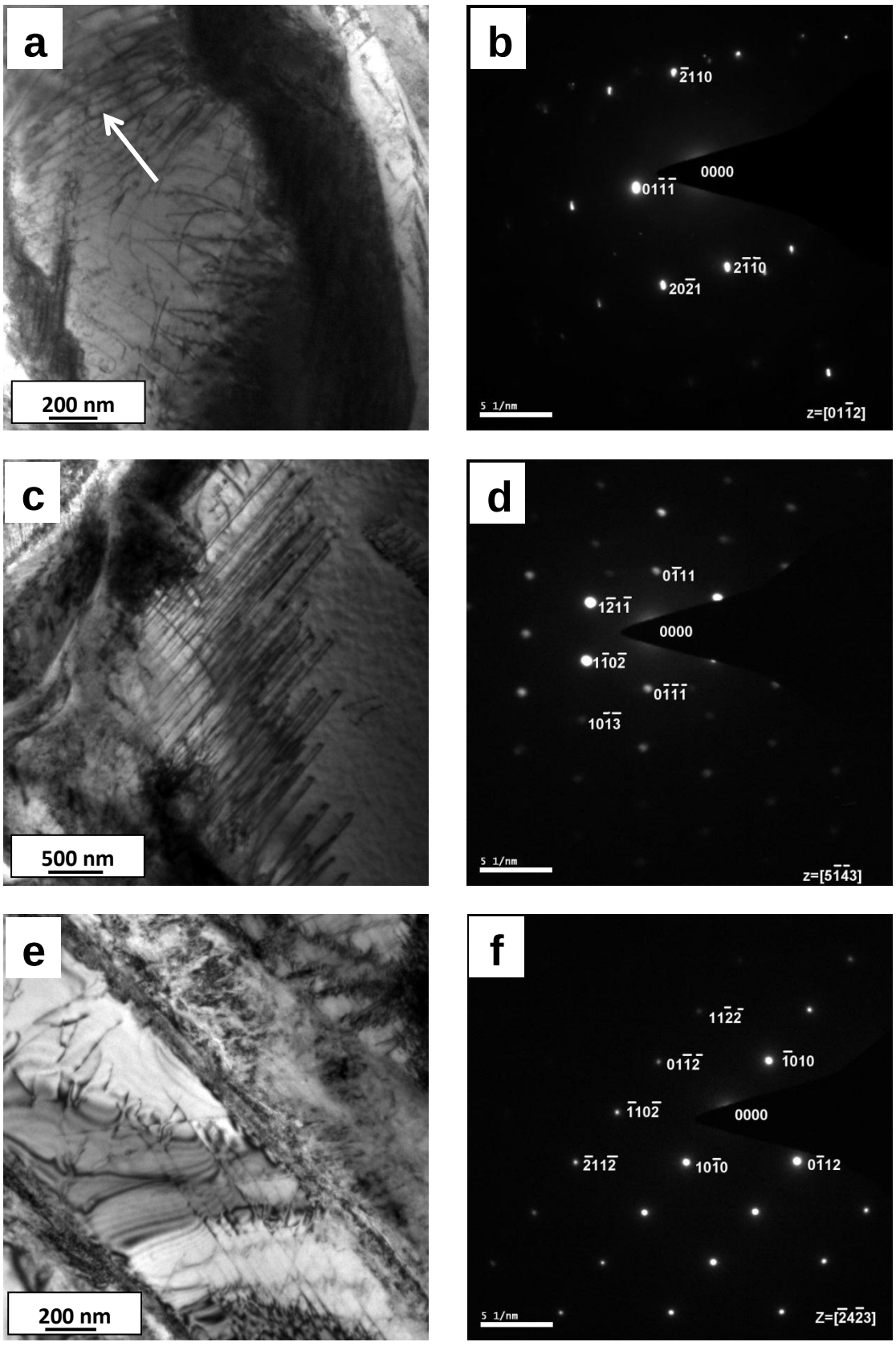

Fig. 6.14 Bright Field TEM micrographs and the corresponding SAD patterns of the specimens tested in LCF at strain amplitude of ±0.60%: (a, b) non-USSPed, (c, d) USSPed and (e, f) USSPed+SR.

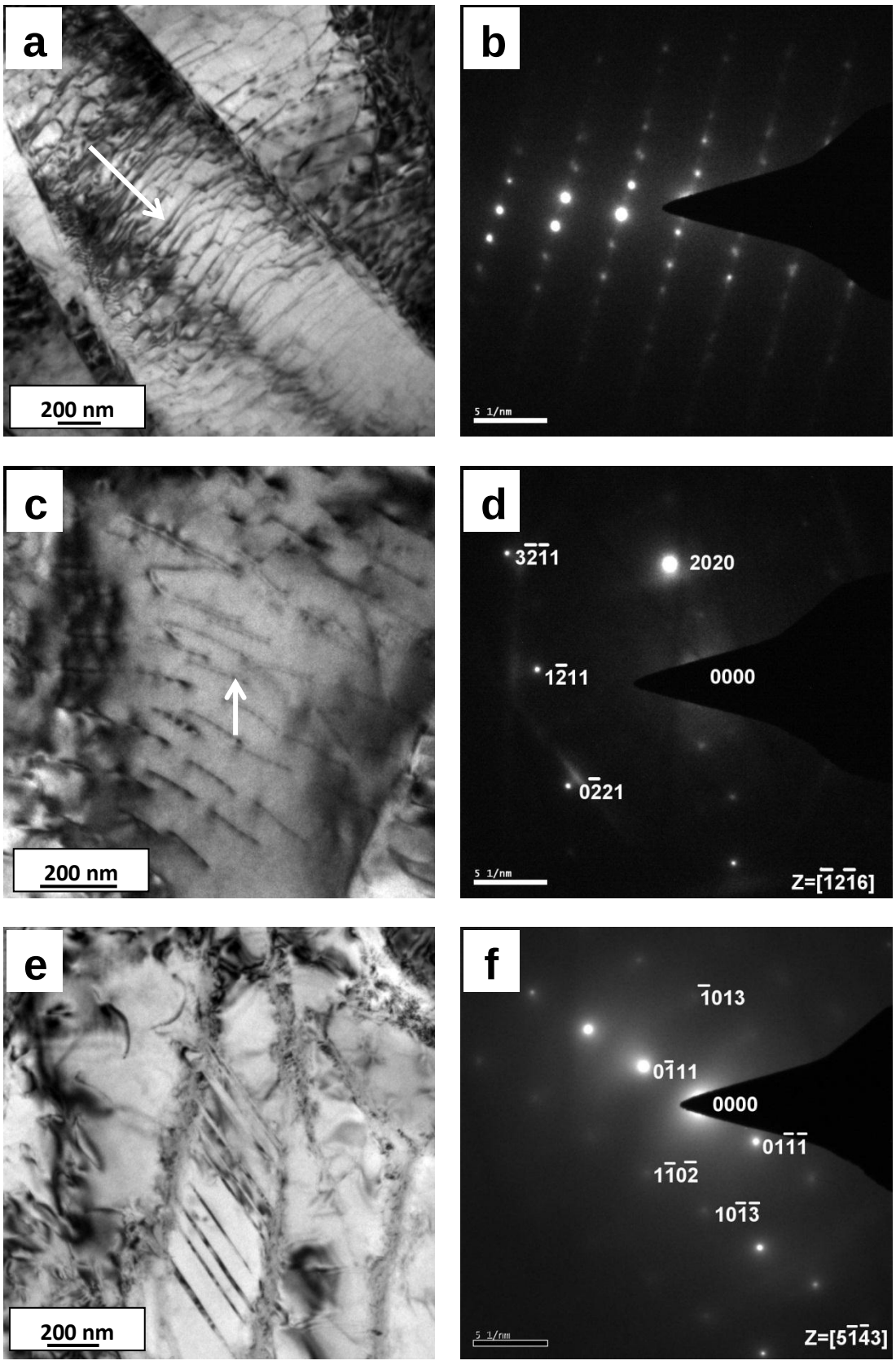

Fig. 6.15 Bright Field TEM micrographs and the corresponding SAD patterns of the specimens tested in LCF at strain amplitude of ±0.65%: (a, b) non-USSPed, (c, d) USSPed and (e, f) USSPed+SR.

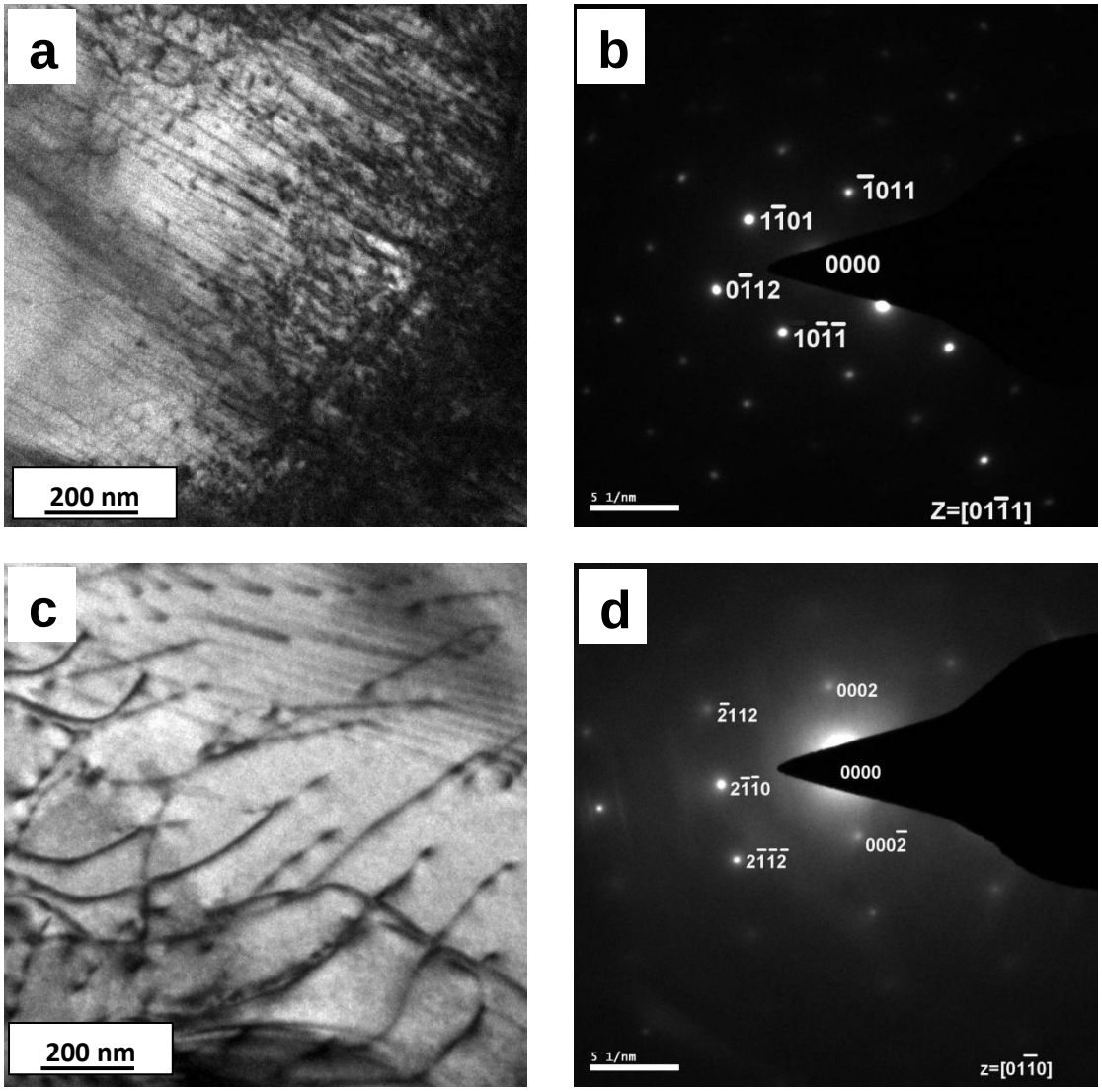

Fig. 6.16 Bright Field TEM micrographs and the corresponding SAD patterns of the specimens tested in LCF at strain amplitude of ±0.70%: (a, b) non-USSPed and (c, d) USSPed samples.

Figure 6.16a shows dislocation tangles at strain amplitude of ±0.70% in non-USSPed sample. However, arrays of dislocations were observed in the α phase for the USSPed sample tested at ±0.70% strain amplitude (Figs. 6.16c). Some fringes were seen in the USSPed sample, tested in LCF at ±0.70% strain amplitude.

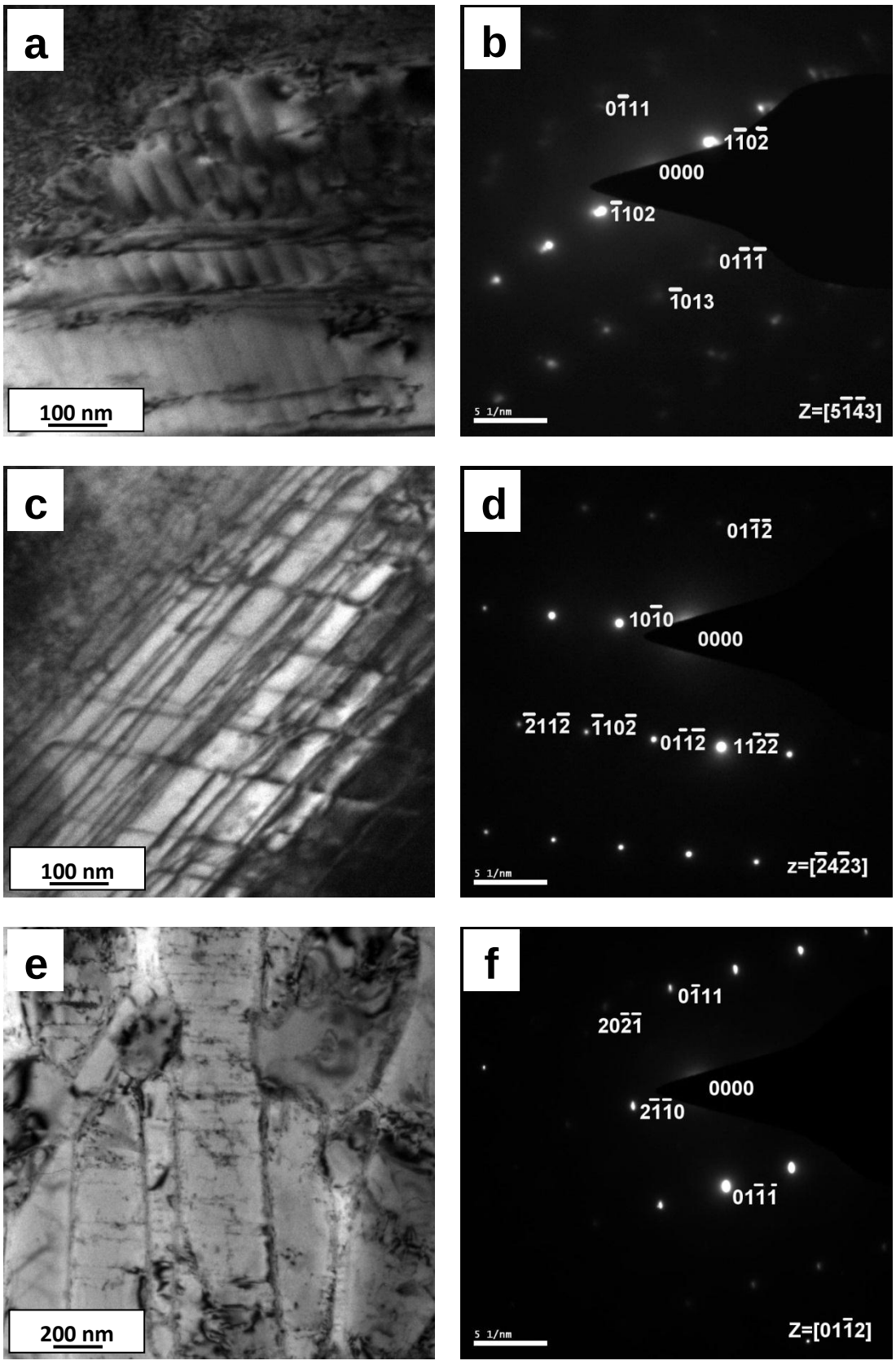

Fig. 6.17 Bright Field TEM micrographs and the corresponding SAD patterns of the specimens tested in LCF at strain amplitude of ±0.80%: (a, b) non-USSPed, (c, d) USSPed and (e, f) USSPed+SR.

There was no evidence of pile-up of dislocations at higher strain amplitude. Arrays planar defects were observed at higher strain amplitude (±0.80%) in secondary α (Fig. 6.17a and 6.17e). There was intersection of two sets of slip bands as indicated by arrow and formation of tiny structure in the region of intersection (Fig. 6.17c).

6.4 DISCUSSION

It is obvious from the present investigation that tensile strength and LCF life was improved from USSP. Tensile strength and yield strength increased with increase in peening treatment time. It was due to enhancement in the resistance to slip due to compressive residual stress and grain refinement in the surface layer. Similar observation of increase in tensile strength was made by Chen et al. (2005) and Roland et al. (2006) in 316L stainless steel from surface nanocrystallization. There was no significant change in the strain hardening exponent (n) due to USSP treatment. Since strain hardening is bulk phenomena and USSP modifies only the surface region of the material the relatively lower work hardening exponent may thus be understood.

Fatigue properties of materials are improved with low surface roughness and favourable compressive residual stress field produced by shot peening [Gao et al. (2004)]. USSP treatment results in lower surface roughness as compared with the other processes of surface treatment. Increase in surface roughness causes strong stress concentration which reduces the effective residual compressive stress on the surface of the shot peened samples [Yan et al. (2010), Feng et al. (2009)].

There was continuous cyclic softening at the higher strain amplitudes (≥±0.75%) in all the cases (Fig. 6.6) which may be attributed to change in the dislocation arrangement to sub-grain and decrease in the dislocation density [Singh et al. (2007),

Rao et al. (2013)]. However, the initial hardening up to 100 cycles may be attributed to increase in dislocation density up to a certain level due to USSP [Llanes et al. 1996), Vinogradov et al. (2007)].

The improvement in fatigue life from the USSP was found to increase with decrease in strain amplitude (Fig. 6.7). Figures 6.8, 6.9, 6.10, 6.11 and 6.12 show fracture surfaces of the non-USSPed, USSPed and USSPed+SR samples tested in LCF and reveal the regions of fatigue crack initiation and propagation. Tire fracture can be seen in Figs. 6.10 (c, d) and 6.12(b). Tire striations are short fatigue striations. The crack initiation sites are marked with arrows. Fatigue cracks are known to initiate from the surface of a component where dislocations slip more easily than at the sub-surface. However, the largest portion of fatigue fracture consists of stage II crack growth exhibiting striations on the fracture surface, and is influenced more by the strain amplitude and microstructure. Fatigue life of the materials is strongly affected by the process of crack initiation and propagation. Number of striations per unit length of fatigue crack propagation was found to be higher on fracture surface of the USSPed specimen than on those of the non-USSPed and USSPed+SR samples.

It may be seen from Fig. 6.13 that N_p is higher than N_i in the non-USSPed and USSPed+SR conditions whereas there is reverse trend in the case of USSPed condition. In the USSPed specimens the difference between N_i and N_p progressively increased with decrease in strain amplitude and N_i may be seen to increase rapidly at the lower strain amplitudes of ±0.65% and ±0.60%. Thus, it is important to mention that enhancement in fatigue life of the USSPed specimens was essentially due to delay in the process of crack initiation and consequent increase in N_i.

Deformation substructures in the non-USSPed, USSPed and USSPed+SR samples tested at different strain amplitudes of ±0.60%, ±0.65%, ±0.70% and ±0.80% are shown in Figs. 6.14, 6.15, 6.16 and 6.17 respectively. It is obvious that dislocations were generated along the interface of the secondary α phase. Dislocation pile-ups were observed on the non-USSPed samples at lower strain amplitude (Fig. 6.14a and 6.15a) resulting from early crack initiation [Prasad et al. (2011)]. It may be seen from Fig. 6.13 that there was early crack initiation in the non-USSPed samples than that in the USSPed one. Individual dislocations were observed during the delayed process of fatigue crack initiation, resulting in increased fatigue life. Singh et al. (2007) studied LCF behaviour of the IMI 834 alloy under strain controlled fatigue at ±0.80% strain amplitude, at room temperature and 873K and individual dislocations were observed in both the conditions but they were relatively less in number in the specimen tested at 873K due to lower fatigue life at high temperature. There were parallel slip bands and intersections of planar slip at higher strain amplitude (Fig. 6.17c) giving rise to continuous softening [Singh et al. (2007)]. Mordyuk et al. (2006) reported that the dislocation movement has little effect when the grain size is in nano scale.

Nikintin et al. (2005) and Vinogradov et al. (2007) reported that there was increase in fatigue life due to nanostructured surface layer in the titanium alloys Ti–6Al–4V and Ti–10V–2Fe–3Al respectively, and it was due to delay in the process of crack initiation and slower crack propagation. USSP produces compressive residual stresses which lower the effective tensile stress at the surface which is highly important for crack initiation and propagation of small cracks through the surface region. Chen et al. (2014) reported that compressive residual stress was induced due to non-uniform

elastic–plastic deformation and lattice distortion caused by the bombardment of shot media against the surface.

Compressive residual stress in the surface region develops from the Hertz dynamic pressure and plastic deformation. The hertz dynamic pressure is dominant and plastic deformation is weak on the material surface when the steel balls impact relatively hard materials [Feng et al. (2009)]. It may be seen that improvement in fatigue life of the USSPed+SR samples was due to grain refinement as the compressive residual stress was reduced by ≈50% after the stress relieving treatment (400°C –1h).

The recent observation of Pandey et al. (2015) in the age hardening 2014 aluminum alloy shows dominant role of grain refinement in enhancing fatigue life, in particular, at the lower strain amplitudes [Singh et al. (2016)]. The enhancement in fatigue life of the near α titanium alloy Timetal 834, having low stacking fault energy, through grain refinement has earlier been demonstrated by Srinadh and Singh (2007) and Tripathi et al. (2013). Thus, the nanostructured surface is observed to play an important role on fatigue life of the alloy Ti–6Al–4V at the lower strain amplitudes.

6.5 CONCLUSIONS

Following conclusions may be drawn from this chapter:

1) Yield and tensile strength increased and ductility decreased with duration of peening.
2) Ductile fracture was observed on tensile tested samples for the non-USSPed and USSPed condition.
3) Cyclic softening was observed at higher strain amplitudes from the beginning, in the alloy Ti–6Al–4V under strain control, at ≥ ±0.75% total strain amplitude.

4) There was significant increase in LCF life, approximately by four times, due to USSP at the lowest strain amplitude.
5) The improvement in fatigue life from USSP was essentially from compressive residual stress, work hardening and grain refinement in the surface region and consequent delay in the process of fatigue crack initiation and propagations.
6) Dislocation pile-ups and planar slip were observed in the non-USSPed and USSPed samples respectively at lower strain amplitude (±0.60).
7) Parallel slip and intersections of planar slip were observed at higher strain amplitude (±0.80) in the both non-USSPed and USSPed samples due to continuous softening till fracture.